Geochimica et Cosmochimica Acta, Vol. 69, No. 24, pp. 5777–5788, 2005

0016-7037/05 $30.00 + .00

doi:10.1016/j.gca.2005.08.011

# Fe-Mg order-disorder in orthopyroxenes

Liping Wang,[1,†] Namdoo Moon,[2] Youxue Zhang,[1,*] William R. Dunham,[2] and Eric J. Essene[1]

[1]Department of Geological Sciences, the University of Michigan, Ann Arbor, MI 48109-1005, USA
[2]Biophysics Research Division, University of Michigan, Ann Arbor, MI 48109, USA

(*Received March* 31, 2005; *accepted in revised form August* 11, 2005)

**Abstract**—Published data on the distribution of Fe and Mg between the two distinct octahedral sites (M1 and M2) in orthopyroxenes show that the equilibrium Fe-Mg distribution coefficient ($K_D$) is roughly constant at intermediate ferrosilite content ($X_{Fs}$ of 0.2 to 0.6) but at low $X_{Fs}$ (<0.2) is either anomalously high (Mössbauer data) or low (XRD data) compared to $K_D$ at intermediate $X_{Fs}$. We report an experimental study on the equilibrium $K_D$ values for two natural single crystals of orthopyroxene (with $X_{Fs}$ of 0.011 and 0.160) using a high-sensitivity Mössbauer spectrometer. The $K_D$ values were determined at 1 bar and temperatures between 600 and 1000°C, and reversed at 600 to 900°C. The values are found to be independent of orthopyroxene composition at a given temperature within analytical uncertainties, and in agreement with $K_D$ values at intermediate $X_{Fs}$. A least-squares fit to the $K_D$ data yields: $\ln K_D = 0.391(\pm 0.131) - 2205(\pm 141)/T$, where $T$ is temperature in K, and uncertainties are at the $2\sigma$ level. This equation is valid for $X_{Fs}$ values up to at least 0.6. We suggest that previous Mössbauer and XRD data at low $X_{Fs}$ were compromised by analytical difficulties. The new result that $K_D$ is roughly independent of $X_{Fs}$ greatly simplifies treatment of equilibrium and speedometry based on Fe-Mg order-disorder in orthopyroxene. *Copyright © 2005 Elsevier Ltd*

## 1. INTRODUCTION

Orthopyroxene is a common mineral in terrestrial rocks and meteorites. There are two common end-members, enstatite (En), $Mg_2Si_2O_6$, and ferrosilite (Fs), $Fe_2Si_2O_6$, which form a solid solution that is stable over a wide range of temperature and pressure. Orthopyroxene has two crystallographically distinct octahedral sites, M1 and M2 in the structure, with $Fe^{2+}$ (referred to as Fe hereafter) preferring the larger and more distorted M2 site and $Mg^{2+}$ (referred to as Mg hereafter) preferring M1 (Ghose, 1965). The Fe-Mg distribution between the two sites is of great interest because of its effect on the thermodynamic property of orthopyroxene and its potential application to the determination of cooling history of terrestrial and extraterrestrial rocks (Ghose and Hafner, 1967; Virgo and Hafner, 1970; Anovitz et al., 1988; Skogby, 1992; Ganguly et al., 1994; Zhang, 1994; Ganguly and Domeneghetti, 1996; Zema et al., 1996; Kroll et al., 1997; Domeneghetti et al., 2000; Heinemann et al., 2000). These applications all rely on a knowledge of equilibrium distribution and exchange kinetics. Hence, considerable effort has been expended to quantify the equilibrium distribution of Mg and Fe between the M1 and M2 sites (Saxena and Ghose, 1971; Ganguly, 1982; Anovitz et al., 1988; Shi et al., 1992; Yang and Ghose, 1994; Kroll et al., 1997; Stimpfl et al., 1999).

The order-disorder reaction of Fe and Mg in orthopyroxene can be described by the following intracrystalline exchange reaction:

$$Fe^{(M2)}Mg^{(M1)}Si_2O_6 = Mg^{(M2)}Fe^{(M1)}Si_2O_6, \quad (1)$$

for which an Fe-Mg distribution coefficient ($K_D$) between M1 and M2 sites can be defined as

$$K_D = \frac{X_{Fe}^{M1} X_{Mg}^{M2}}{X_{Fe}^{M2} X_{Mg}^{M1}}, \quad (2)$$

where for instance $X_{Fe}^{M1}$ is the mole fraction of Fe in the M1 site. The intracrystalline Fe-Mg distribution and the kinetics of the order-disorder reaction for natural and synthetic orthopyroxenes have been extensively investigated for intermediate ferrosilite contents ($X_{Fs}$ of 0.2 to 0.8, where $X_{Fs}$ refers to the mole fraction of ferrosilite component) using Mössbauer spectroscopy (MS) and single-crystal X-ray diffraction (XRD) techniques (Virgo and Hafner, 1969; Saxena and Ghose, 1971; Besancon, 1981; Anovitz et al., 1988; Saxena et al., 1989; Molin et al., 1991; Skogby, 1992; Yang and Ghose, 1994; Kroll et al., 1997; Stimpfl et al., 1999; Schlenz et al., 2001; Zema et al., 2003). The most relevant compositions for an orthopyroxene from the terrestrial upper mantle and many meteorites are however, in the range of $0 < X_{Fs} < 0.2$. The few data that are available for $X_{Fs} < 0.2$ suggest a strong compositional dependence of $K_D$ (e.g., Skogby, 1992; Kroll et al., 1997; Stimpfl et al., 1999). These results are unexpected since $K_D$ would normally be expected to be less compositionally dependent at low $X_{Fs}$ (i.e., following the application of Raoult's Law and Henry's Law to Eqn. 2. The uncertainty of determining Fe in M1 site increases with decreasing $X_{Fs}$ for both MS and XRD techniques, making it impossible to reliably extrapolate to magnesian orthopyroxenes (Kroll et al., 1997). Thus, a better constraint on Fe-Mg order-disorder in orthopyroxene with low $X_{Fs}$ will contribute to a deeper understanding of this problem. Here we report results from an experimental investigation of Fe-Mg distribution between M1 and M2 sites in two magnesian orthopyroxenes with $X_{Fs}$ of 0.011 and 0.16.

* Author to whom correspondence should be addressed (youxue@umich.edu).
† *Present address:* Mineral Physics Institute, State University of New York at Stony Brook, Stony Brook, NY 11794-2100, USA.

## 2. SAMPLE DESCRIPTION AND PREPARATION

Two natural single crystals of orthopyroxene, En-LMA and En-82161, were used in the current study. Sample En-LMA (~ 15 g) was kindly provided by L.M. Anovitz at the Oak Ridge National Laboratory, and sample En-82161 (~ 0.8 g) by the American Museum of Natural History at New York (AMNH#82161). Sample En-LMA was purchased at the Tucson Mineral Show, and was stated by the seller to be from Zabargad Island in the Red Sea. It is clouded by minute magnesite and talc inclusions (< 100 $\mu$m across) in some regions and along cleavages as seen in a thin section of the sample. Electron microprobe analyses show that both talc and magnesite contain only very small amounts of Fe (< 0.1 wt% FeO), which means that that small amounts of inclusions will not contribute materially to the Mössbauer signal. Sample En-82161 is inclusion-free but has hematite staining on cleavage surfaces. Neither sample showed any exsolution features visible in back-scattered electron images in a scanning electron microscope. The crystals were cut and crushed, and final samples were handpicked to ensure that only gem-quality material free of inclusions was used for the experiments. The hematite staining was removed by washing the sample in 2 N nitric acid in an ultrasonic bath. Powder XRD studies on final samples revealed only peaks of orthopyroxene.

Magnesian orthopyroxene grains from each handpicked sample pool were mounted, polished and analyzed on a four-spectrometer Cameca Camebax electron microprobe at the University of Michigan using an accelerating voltage of 15 kV with a focused current of 10 nA. Counting times of 30 s or total counts of 40,000 were used for all elements in standards and samples. The analytical data were corrected using the Cameca PAP program. The average composition of each sample is reported in Table 1. Each crystal used in this study is homogeneous within 10% relative in terms of FeO content.

Table 1. Electron microprobe analyses of orthopyroxenes.

| Sample | En-LMA ($n$ = 47) | En-82161 ($n$ = 38) |
|---|---|---|
| $SiO_2$ | 58.96 (0.59)[a] | 56.52 (0.76) |
| $TiO_2$ | 0.03 (0.04) | 0.02 (0.04) |
| $Al_2O_3$ | 0.90 (0.31) | 0.50 (0.12) |
| $Cr_2O_3$ | 0.01 (0.03) | 0.05 (0.05) |
| FeO[b] | 0.76 (0.12) | 10.86 (1.13) |
| MnO | 0.02 (0.04) | 0.22 (0.10) |
| MgO | 39.07 (0.48) | 31.49 (0.83) |
| CaO | 0.04 (0.02) | 0.27 (0.05) |
| $Na_2O$ | 0.01 (0.01) | 0.01 (0.02) |
| Total | 99.79 (0.81) | 99.94 (0.60) |
| | Formulae based on four cations[c] | |
| Si | 1.982 (0.012) | 1.989 (0.018) |
| Al | 0.036 (0.012) | 0.021 (0.005) |
| $^{IV}$Al | 0.018 | 0.011 |
| $^{VI}$Al | 0.017 | 0.009 |
| Ti | 0.0007 (0.0009) | 0.0006 (0.0009) |
| Cr | 0.0002 (0.0007) | 0.0015 (0.0015) |
| Mg | 1.958 (0.018) | 1.651 (0.037) |
| Fe | 0.021 (0.003) | 0.320 (0.035) |
| $Fe^{3+}$ | 0 | 0 |
| $Fe^{2+}$ | 0.021 | 0.320 |
| Ca | 0.0016 (0.0007) | 0.010 (0.002) |
| Mn | 0.0005 (0.0012) | 0.007 (0.003) |
| Na | 0.0004 (0.0009) | 0.0007 (0.0013) |
| O (calc.) | 6.000 (0.013) | 6.000 (0.017) |

[a] Numbers in parentheses are two times standard deviations ($2\sigma$) for the corresponding oxide concentration. They include contributions from uncertainties in microprobe analyses and sample heterogeneities.
[b] Total Fe as FeO.
[c] Most probable formula (calculated by J. Ganguly) is consistent with the calculated formula shown, with differences in the fourth decimal place. The resulting different in $\ln K_D$ is also in the fourth decimal place and hence negligible.

## 3. EXPERIMENTAL AND ANALYTICAL METHODS

### 3.1. Heating Experiments

A horizontal tube furnace was used in the heating experiments. The furnace was equipped with an automatic temperature controller and lined with a silica glass tube through which dry $N_2$ gas could be passed during the heating. The controlling thermocouple (Platinel-II: $Pt_{35}Au_{65}/Pt_{17}Pd_{83}$) was outside the silica tube and a second thermocouple (Type-S: $Pt/Pt_{90}Rh_{10}$) was inside the silica tube to record the experimental temperature. The inside thermocouple was calibrated against the melting point of gold. The accuracy of the reported temperature is ± 2°C. The furnace was always preheated to the desired temperatures indicated by the inside thermocouple before inserting the sample. When the sample assemblage was placed in the hot spot in contact with the tip of the thermocouple, the temperature reading initially decreased by up to 30°C, but a steady temperature was reached in less than 2 min. The exact time depends on the size of the sample holder. For some kinetic experiments of very short duration, the sample was wrapped by thermocouple wires and temperature recovery occurred in seconds. The temperature fluctuation over the course of each heating experiment was ± 1°C.

Samples consisting of 1–2-mm-sized orthopyroxene grains were loaded into a silica boat or tube, fenced by quartz wool to one end of the container, and placed in the preheated furnace with a continuous $N_2$ flow (manufacture specification: 99.998% purity, with ~10 ppm $O_2$). Experiments were conducted at 1 atm total pressure and temperatures of 600 to 1000°C, with run times ranging from minutes at 900 to 1000°C to ~1 month at 600°C (Table 2). At the end of each heat treatment, the container was removed from the furnace, and dropped in water or placed on the lab bench to cool, depending on the quenching rate needed to preserve the ordering state. The quench rate in water is of the order of hundreds of K/s, and that in air is 10–20 K/s (Xu and Zhang, 2002). Powder XRD patterns were obtained for several samples heated at 600 and 1000°C, and no phase change was detected.

For equilibrium experiments, experimental reversals were achieved to constrain the equilibrium state at temperatures of 600 to 900°C using natural ordered and experimentally disordered samples. Disordered materials were prepared by heating a portion of each sample pool at 1000°C for an hour following the procedure described above. No reversal was attempted at 1000°C because a more disordered state cannot be preserved upon quenching.

### 3.2. Mössbauer Analysis and Data Reduction

A wide-angle Mössbauer spectrometer at the Biophysics Research Division at the University of Michigan was employed to analyze the experimental products.[1] The instrument was designed to study iron substitution in proteins. Its structural details and the data collection procedure have been described elsewhere (Moon et al., 1996) and will only be summarized here. The most innovative feature of the spectrometer is the eighty-degree, conical acceptance geometry of its $\gamma$-ray detector, which consists of 77 argon gas proportional counters. Compared to a conventional Mössbauer spectrometer (i.e., single counter), the new instrument has the following advantages: (i) a count rate ~100 times that of a conventional spectrometer; (ii) a sensitivity ~10 times better than that of a conventional spectrometer; (iii) high reproducibil-

[1] This Mössbauer spectrometer was decommissioned in 2001 with the retirement of William R. Dunham.

Table 2. Experimental details and Fe-Mg distribution coefficients.

| No. | Starting sample[a] | $T$ (°C) | Duration (min) | Area ratio (M1/M2) | $X_{Fe}$ (M1) | $X_{Mg}$ (M1) | $X_{Fe}$ (M2) | $X_{Mg}$ (M2) | $\ln K_D$ |
|---|---|---|---|---|---|---|---|---|---|
| | | | | Sample En-LMA | | | | | |
| 1 | NS | no heating | | 0.1017 (34)[b] | 0.00197 (6) | 0.9797 | 0.0194 | 0.9780 | |
| 1a | NS | no heating | | 0.1060 (44) | 0.00205 (8) | 0.9796 | 0.0193 | 0.978 | |
| 79 | NS | no heating | | 0.1012 (66) | 0.00196 (11) | 0.9797 | 0.0194 | 0.9779 | |
| | Average | natural | | 0.1030 (52) | 0.00199 (9) | 0.9797 | 0.0194 | 0.9780 | −2.275 (51) |
| 80 | NS | 1000 | 10 | 0.2636 (61) | 0.00446 (8) | 0.9772 | 0.0169 | 0.9804 | −1.330 (23) |
| 5 | NS | 1000 | 90 | 0.2412 (49) | 0.00415 (7) | 0.9775 | 0.0172 | 0.9801 | −1.420 (20) |
| 6 | NS[c] | 1000 | 90 | 0.2752 (48) | 0.00461 (6) | 0.9770 | 0.0167 | 0.9806 | −1.287 (18) |
| 2 | NS | 1000 | 150 | 0.2540 (48) | 0.00433 (6) | 0.9773 | 0.0170 | 0.9803 | −1.367 (19) |
| | Average | 1000 | | | | | | | −1.350 (113) |
| 45 | DO[c] | 900 | 0.17 | 0.2354 (80) | 0.00409 (11) | 0.9776 | 0.0173 | 0.9801 | |
| 46 | DO[c] | 900 | 0.50 | 0.2259 (49) | 0.00394 (7) | 0.9777 | 0.0174 | 0.9799 | |
| 41 | DO | 900 | 2 | 0.2153 (41) | 0.00378 (6) | 0.9779 | 0.0176 | 0.9798 | −1.534 (19) |
| 43 | DO | 900 | 5 | 0.2148 (40) | 0.00378 (6) | 0.9779 | 0.0176 | 0.9798 | −1.536 (19) |
| 3 | DO | 900 | 30 | 0.2307 (49) | 0.00400 (7) | 0.9776 | 0.0174 | 0.9800 | −1.464 (22) |
| 9 | DO[c] | 900 | 60 | 0.2347 (45) | 0.00406 (6) | 0.9776 | 0.0173 | 0.9800 | −1.447 (19) |
| 4 | DO | 900 | 90 | 0.2280 (45) | 0.00397 (6) | 0.9777 | 0.0174 | 0.9799 | −1.476 (20) |
| 55 | NS | 900 | 0.25 | 0.0803 (41) | 0.00159 (8) | 0.9801 | 0.0198 | 0.9775 | |
| 47 | NS | 900 | 0.50 | 0.0686 (41) | 0.00137 (8) | 0.9803 | 0.0200 | 0.9774 | |
| 56 | NS | 900 | 0.75 | 0.0697 (43) | 0.00139 (8) | 0.9803 | 0.0200 | 0.9774 | |
| 57 | NS | 900 | 1.08 | 0.0910 (38) | 0.00178 (7) | 0.9799 | 0.0196 | 0.9778 | |
| 64 | NS | 900 | 1.67 | 0.2106 (72) | 0.00372 (11) | 0.9779 | 0.0176 | 0.9797 | |
| 42 | NS | 900 | 2 | 0.2189 (41) | 0.00384 (6) | 0.9778 | 0.0175 | 0.9798 | −1.517 (19) |
| 44 | NS | 900 | 5 | 0.2219 (60) | 0.00388 (9) | 0.9778 | 0.0175 | 0.9799 | −1.503 (27) |
| 7 | NS | 900 | 20 | 0.2376 (48) | 0.00410 (7) | 0.9775 | 0.0173 | 0.9801 | −1.435 (20) |
| 8 | NS | 900 | 60 | 0.2314 (36) | 0.00401 (5) | 0.9776 | 0.0173 | 0.9800 | −1.461 (16) |
| 10 | NS[c] | 900 | 60 | 0.2367 (55) | 0.00409 (8) | 0.9776 | 0.0173 | 0.9801 | −1.438 (23) |
| | Average | 900 | | | | | | | −1.481 (77) |
| 11 | DO | 800 | 5 | 0.2012 (43) | 0.00358 (6) | 0.9781 | 0.0178 | 0.9796 | |
| 35 | DO | 800 | 10 | 0.1926 (55) | 0.00345 (8) | 0.9782 | 0.0179 | 0.9794 | −1.646 (29) |
| 13 | DO | 800 | 20 | 0.1787 (63) | 0.00324 (10) | 0.9784 | 0.0181 | 0.9792 | −1.722 (35) |
| 37 | DO | 800 | 40 | 0.1911 (41) | 0.00343 (6) | 0.9782 | 0.0179 | 0.9794 | −1.654 (22) |
| 16 | DO | 800 | 60 | 0.1888 (50) | 0.00339 (8) | 0.9783 | 0.0180 | 0.9794 | −1.666 (27) |
| 62 | NS | 800 | 0 | 0.1055 (39) | 0.00204 (7) | 0.9796 | 0.0193 | 0.9780 | |
| 63 | NS | 800 | 0.42 | 0.0798 (37) | 0.00158 (7) | 0.9801 | 0.0198 | 0.9776 | |
| 58 | NS | 800 | 0.67 | 0.0732 (34) | 0.00146 (6) | 0.9802 | 0.0199 | 0.9774 | |
| 59 | NS | 800 | 1.33 | 0.0781 (42) | 0.00155 (8) | 0.9801 | 0.0198 | 0.9775 | |
| 60 | NS | 800 | 2 | 0.0819 (41) | 0.00162 (8) | 0.9800 | 0.0197 | 0.9776 | |
| 61 | NS | 800 | 3 | 0.1130 (37) | 0.00217 (6) | 0.9795 | 0.0192 | 0.9781 | |
| 12 | NS | 800 | 5 | 0.1617 (35) | 0.00297 (5) | 0.9787 | 0.0184 | 0.9790 | |
| 36 | NS | 800 | 10 | 0.1913 (44) | 0.00343 (7) | 0.9782 | 0.0179 | 0.9794 | −1.653 (23) |
| 14 | NS | 800 | 20 | 0.1881 (47) | 0.00338 (7) | 0.9783 | 0.0180 | 0.9794 | −1.670 (25) |
| 38 | NS | 800 | 40 | 0.1871 (52) | 0.00337 (8) | 0.9783 | 0.0180 | 0.9793 | −1.675 (28) |
| 15 | NS | 800 | 60 | 0.1946 (43) | 0.00348 (6) | 0.9782 | 0.0179 | 0.9795 | −1.636 (22) |
| | Average | 800 | | | | | | | −1.665 (53) |
| 18 | DO | 700 | 10 | 0.2339 (52) | 0.00405 (7) | 0.9776 | 0.0173 | 0.9800 | |
| 20 | DO | 700 | 50 | 0.2112 (47) | 0.00373 (7) | 0.9779 | 0.0176 | 0.9797 | |
| 27 | DO | 700 | 100 | 0.1738 (43) | 0.00316 (7) | 0.9785 | 0.0182 | 0.9791 | |
| 28 | DO | 700 | 205 | 0.1854 (51) | 0.00334 (8) | 0.9783 | 0.0180 | 0.9793 | |
| 31 | DO | 700 | 360 | 0.1553 (17) | 0.00287 (3) | 0.9788 | 0.0185 | 0.9789 | −1.862 (11) |
| 33 | DO | 700 | 610 | 0.1447 (44) | 0.00270 (7) | 0.9790 | 0.0187 | 0.9787 | −1.934 (31) |
| 81 | DO | 700 | 900 | 0.1556 (49) | 0.00288 (8) | 0.9788 | 0.0185 | 0.9789 | −1.860 (32) |
| 21 | NS | 700 | 5 | 0.0720 (47) | 0.00143 (9) | 0.9802 | 0.0199 | 0.9774 | |
| 17 | NS | 700 | 10 | 0.0802 (40) | 0.00159 (7) | 0.9801 | 0.0198 | 0.9776 | |
| 29 | NS | 700 | 15 | 0.0787 (40) | 0.00156 (7) | 0.9801 | 0.0198 | 0.9775 | |
| 22 | NS | 700 | 21 | 0.1014 (44) | 0.00197 (8) | 0.9797 | 0.0194 | 0.9779 | |
| 23 | NS | 700 | 35 | 0.1084 (47) | 0.00209 (8) | 0.9796 | 0.0193 | 0.9781 | |
| 19 | NS | 700 | 50 | 0.1191 (46) | 0.00227 (8) | 0.9794 | 0.0191 | 0.9783 | |
| 25 | NS | 700 | 100 | 0.1261 (43) | 0.00239 (7) | 0.9793 | 0.0190 | 0.9784 | |
| 26 | NS | 700 | 200 | 0.1663 (44) | 0.00305 (7) | 0.9786 | 0.0183 | 0.9790 | |
| 30 | NS | 700 | 360 | 0.1422 (46) | 0.00266 (8) | 0.9790 | 0.0187 | 0.9786 | −1.951 (33) |
| 34 | NS | 700 | 610 | 0.1508 (48) | 0.00280 (8) | 0.9789 | 0.0186 | 0.9788 | −1.892 (32) |
| 82 | NS | 700 | 900 | 0.1611 (50) | 0.00296 (8) | 0.9787 | 0.0184 | 0.9789 | −1.825 (31) |
| | Average | 700 | | | | | | | −1.887 (95) |
| 48 | DO | 600 | 600 | 0.2361 (46) | 0.00408 (6) | 0.9776 | 0.0173 | 0.9801 | |
| 49 | DO | 600 | 1920 | 0.2151 (82) | 0.00378 (12) | 0.9779 | 0.0176 | 0.9798 | |
| 50 | DO | 600 | 3720 | 0.1898 (50) | 0.00341 (8) | 0.9782 | 0.0180 | 0.9794 | |

Table 2. (Continued)

| No. | Starting sample[a] | $T$ (°C) | Duration (min) | Area ratio (M1/M2) | $X_{Fe}$ (M1) | $X_{Mg}$ (M1) | $X_{Fe}$ (M2) | $X_{Mg}$ (M2) | $\ln K_D$ |
|---|---|---|---|---|---|---|---|---|---|
| 51 | DO | 600 | 6000 | 0.1771 (53) | 0.00321 (8) | 0.9784 | 0.0181 | 0.9792 | |
| 52 | DO | 600 | 11760 | 0.1487 (50) | 0.00276 (8) | 0.9789 | 0.0186 | 0.9787 | |
| 54 | DO | 600 | 20300 | 0.1534 (71) | 0.00284 (11) | 0.9788 | 0.0185 | 0.9788 | |
| 65 | DO | 600 | 29700 | 0.1444 (57) | 0.00269 (9) | 0.9790 | 0.0187 | 0.9787 | |
| 72 | DO | 600 | 48165 | 0.1239 (56) | 0.00236 (10) | 0.9793 | 0.0190 | 0.9783 | −2.089 (46) |
| 67 | NS | 600 | 15 | 0.0868 (35) | 0.00171 (6) | 0.9799 | 0.0197 | 0.9777 | |
| 68 | NS | 600 | 30 | 0.0845 (31) | 0.00166 (6) | 0.9800 | 0.0197 | 0.9776 | |
| 69 | NS | 600 | 45 | 0.0820 (37) | 0.00162 (7) | 0.9800 | 0.0197 | 0.9776 | |
| 70 | NS | 600 | 60 | 0.0728 (52) | 0.00145 (10) | 0.9802 | 0.0199 | 0.9774 | |
| 71 | NS | 600 | 90 | 0.0688 (44) | 0.00138 (8) | 0.9803 | 0.0200 | 0.9774 | |
| 74 | NS | 600 | 120 | 0.0724 (59) | 0.00144 (11) | 0.9802 | 0.0199 | 0.9774 | |
| 75 | NS | 600 | 180 | 0.0713 (39) | 0.00142 (7) | 0.9802 | 0.0199 | 0.9774 | |
| 76 | NS | 600 | 540 | 0.0964 (45) | 0.00188 (8) | 0.9788 | 0.0195 | 0.9779 | |
| 73 | NS | 600 | 48165 | 0.1113 (41) | 0.00214 (7) | 0.9795 | 0.0192 | 0.9781 | −2.197 (37) |
| 73a[d] | NS | 600 | 48165 | 0.1015 (71) | 0.00197 (12) | 0.9797 | 0.0194 | 0.9779 | −2.289 (70) |
| Average | | 600 | | | | | | | −2.143 (153) |
| | | | | Sample En-82161 | | | | | |
| 77 | no heating | | | 0.0545 (34) | 0.0165 (10) | 0.9720 | 0.3028 | 0.6797 | |
| 77a | no heating | | | 0.0515 (24) | 0.0156 (07) | 0.9728 | 0.3037 | 0.6789 | |
| | NS (2 analyses) | | | 0.0530 (42) | 0.0161 (12) | 0.9724 | 0.3033 | 0.6793 | −3.297 (82) |
| 83 | NS[c] | 1000 | 10 | 0.2732 (57) | 0.0685 (11) | 0.9200 | 0.2508 | 0.7318 | −1.526 (24) |
| 95 | NS[c] | 1000 | 20 | 0.3013 (44) | 0.0739 (08) | 0.9145 | 0.2454 | 0.7372 | −1.415 (16) |
| Average | | 1000 | | | | | | | −1.471 (157) |
| 85 | NS[c] | 900 | 25 | 0.2793 (51) | 0.0697 (10) | 0.9188 | 0.2496 | 0.7330 | −1.502 (21) |
| 84 | DO[c] | 900 | 25 | 0.2656 (58) | 0.0670 (12) | 0.9215 | 0.2523 | 0.7303 | −1.558 (25) |
| 94 | NS[c] | 900 | 40 | 0.2917 (47) | 0.0721 (09) | 0.9164 | 0.2472 | 0.7353 | −1.452 (18) |
| 93 | DO[c] | 900 | 40 | 0.2839 (43) | 0.0706 (08) | 0.9179 | 0.2487 | 0.7339 | −1.483 (17) |
| Average | | 900 | | | | | | | −1.499 (89) |
| 87 | NS | 800 | 40 | 0.2332 (55) | 0.0604 (12) | 0.9281 | 0.2590 | 0.7236 | −1.705 (26) |
| 86 | DO | 800 | 40 | 0.2416 (48) | 0.0621 (10) | 0.9263 | 0.2572 | 0.7254 | −1.665 (22) |
| 92 | NS | 800 | 70 | 0.2450 (44) | 0.0628 (09) | 0.9257 | 0.2565 | 0.7261 | −1.649 (20) |
| Average | | 800 | | | | | | | −1.673 (57) |
| 89 | NS | 700 | 780 | 0.2033 (41) | 0.0540 (09) | 0.9345 | 0.2654 | 0.7172 | −1.858 (23) |
| 88 | DO | 700 | 780 | 0.2023 (63) | 0.0537 (14) | 0.9348 | 0.2656 | 0.7170 | −1.863 (34) |
| Average | | 700 | | | | | | | −1.861 (08) |
| 91 | NS | 600 | 13200 | 0.1712 (42) | 0.0467 (10) | 0.9418 | 0.2727 | 0.7099 | −2.048 (27) |
| 90 | DO | 600 | 13200 | 0.1467 (77) | 0.0409 (19) | 0.9476 | 0.2785 | 0.7041 | −2.217 (57) |
| Average | | 600 | | | | | | | −2.132 (239) |

[a] Starting sample: NS = natural ordered sample (disordered during experiment); DO = experimentally disordered sample.
[b] Uncertainties at $2\sigma$ level for the area ratio are given in parentheses. 0.0530(42) means 0.0530 ± 0.0042. When $\ln K_D$ values are not given, it means that the experiment is a kinetic experiment and has not reached equilibrium.
[c] Sample quenched in water after heating; others quenched in air.
[d] Half of absorber for Run 73 was ground, remixed with boric acid, and rerun Mössbauer analysis. This data point has lower precision than others.

ity of velocity (to an accuracy of ± 0.005 mm/s over periods of several weeks); and (iv) high accuracy in regulating the temperatures of the source and the sample (to ± 1°C). These features allow accurate assessment of the Fe distributions of orthopyroxene that are quite low in Fe (e.g., sample En-LMA, $X_{Fs} = 0.011$), and the use of an exceedingly small amount of sample (in terms of effective thickness of Fe), impossible for a conventional Mössbauer spectrometer.

The Mössbauer absorbers were prepared by mixing the finely powdered orthopyroxene with ~420 mg of boric acid powder and pressing into a disk with a diameter of 1.62 cm and a thickness of ~1.65 mm. The amount of orthopyroxene used was 50–100 mg for sample En-LMA and 5–10 mg for sample En-82161. The average absorber thickness calculated assuming uniform distribution of sample in the absorber was 0.15–0.44 mg Fe/cm$^2$, with most of runs having a thickness of 0.30 mg Fe/cm$^2$ or less. A 35 mCi $^{57}$Co in 6-$\mu$m Rh source and a velocity scan range of ~8.9 mm/s (-4.4 to 4.5 mm/s) were used during Mössbauer measurements. Samples were run in transmission mode for 20–48 h, depending on the absorber thickness. Typically, a sample with a thickness of 0.30 mg Fe/cm$^2$ was run for 24 h. The velocity scale was calibrated relative to pure $\alpha$-Fe foil (NBS #1541). During Mössbauer analyses, samples were cooled using liquid $N_2$ and the temperature was regulated to 125 K, which is the lowest temperature achievable to avoid severe attenuation of gamma rays by liquid $N_2$ in the beam path. In response to comments by a reviewer to an earlier version of this paper, Mössbauer analyses for two run products (#94 and #95) were carried out at three temperatures: 125 K, 175 K and 225 K to investigate the recoil-free fractions of Fe in M1 and M2 sites.

A typical Mössbauer spectrum is shown in Figure 1 (Wang , 1999). There are four peaks: two at low velocity (~0 mm/s), and two at high velocity (~2.2 mm/s). The two large peaks (one at low velocity and one at high velocity), also the two inner peaks, are due to Fe in M2; and the two small peaks (also the two outer peaks) on the shoulders of the larger M2 peaks are due to Fe in M1. A persistent feature for all spectra is the asymmetry of quadruple doublets, namely, the unequal amplitude and width for the two components of M2 doublet. This feature was also observed in previous studies on orthopyroxene (Virgo and Hafner, 1969; Burnham et al., 1971; Saxena and Ghose, 1971; Anovitz et al., 1988; Domeneghetti and Steffen, 1992; Angel et al., 1998). There are three known causes for such asymmetry. One cause, usually referred to as the next-nearest neighbor (NNN) effect, or the statistical hyperfine parameter distribution, is due to short range ordering around the Mössbauer nucleus (e.g., Rancourt, 1989), and has been identified in orthopyroxene (e.g., Seifert, 1983; Angel et al., 1998). This effect results in inhomogeneous line broadening and hence asymmetry in amplitude,

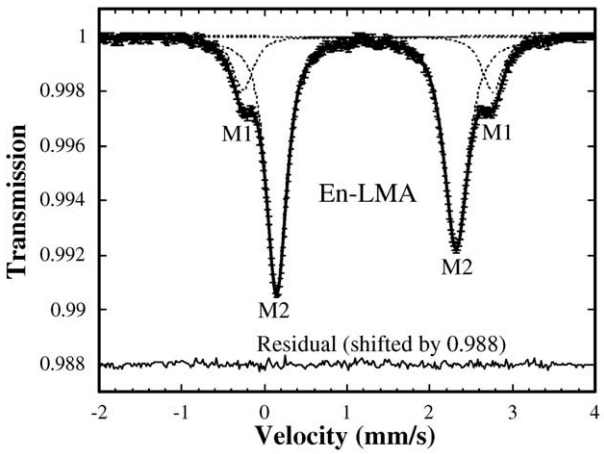


Fig. 1. Representative Mössbauer spectrum for low-Fe orthopyroxene sample (En-LMA, run #10, 900°C, 60 min, Table 2). The solid curve is a fit to the spectrum, and the dashed curves are individual lines. The residual is also shown (shifted upward by 0.988 units for clarity).

but the equality of area intensity of doublet is preserved for a randomly oriented powder absorber. The area intensities of low- and high-velocity components of each doublet in this study differ much less than the peak heights. We hence conclude that the statistical distribution of hyperfine parameters is the dominant factor in causing the amplitude asymmetry. The second cause, usually referred to as the texture effect, is the preferred orientation of mineral grains, such as alignment along a cleavage plane (e.g., Rancourt, 1989). This effect results in unequal intensity in both amplitude and area of the doublet. This effect was tested with natural ordered samples prepared in two different ways. One is to loosely place sample powders in a holder with no binder and no compression. The other is to crush powders to smaller grains. In both cases, compared to samples prepared following the usual procedure described in the preceding section, the doublet asymmetry remained and the magnitude of the asymmetry did not change significantly. Hence we conclude that the texture effect is not an important contributor to the asymmetry. The third cause, referred to as the Goldanskii-Karyagin effect, is caused by the vibrational anisotropy of the Mössbauer nucleus (e.g., Hawthorne, 1988; Rancourt, 1989). This effect results in doublet asymmetry similar to that caused by the texture effect, and it is difficult to separate two effects (Hawthorne, 1988). In the present study, the minor asymmetry in peak area could be due to the texture effect, the Goldanskii-Karyagin effect, or a combination of both. The temperature dependence of line symmetry cannot be clearly resolved by collection of data at different temperatures. Fortunately, the asymmetry is not a critical issue for the determination of equilibrium and kinetic constants.

Mössbauer spectra were fit to four singlets using the commercially available PeakFit program (SPSS Inc., Chicago, Illinois, USA), with the outer two peaks corresponding to Fe in the M1 sites and the inner two to Fe in the M2 sites (Fig. 1). Each peak was simulated by a combination of Lorentzian and gaussian line shapes. Widths of the two Fe(M1) peaks are not well resolved because the peaks are weak and overlap with the strong Fe(M2) peaks. The Fe(M1) peak widths obtained from the fit may vary substantially from one spectrum to the next, resulting in large uncertainties in unconstrained fits for repeated experiments under the same experimental conditions. To mitigate this problem, we applied an additional constraint. From the unconstrained fits, it is apparent that the width of each Fe(M1) peak is roughly the same as that of its adjacent Fe(M2) peak. Reproducible $X_{Fe}^{M1}/X_{Fe}^{M2}$ ratios were obtained if the width of each Fe(M1) peak is assumed to be identical to that of its adjacent Fe(M2) peak (that is, the low-velocity M1 has the same width as the low-velocity M2 peak, and the same for the high-velocity M1 and M2 peaks). Although there is no theoretical basis for this constraint, comparison with two other fitting techniques showed that all fittings yielded consistent results within uncertainties. Hence, the width constraint was used for all fits. The resultant average isomer shift ($\delta$; relative to pure $\alpha$-Fe) and quadruple splitting ($\Delta E_q$) are 1.247 ± 0.009 and 3.010 ± 0.018 mm/s for M1 site and 1.232 ± 0.003 and 2.161 ± 0.006 mm/s for M2 site for sample En-LMA, and 1.248 ± 0.013 and 2.972 ± 0.026 mm/s for M1 site and 1.229 ± 0.012 and 2.137 ± 0.024 mm/s for M2 site for sample En-82161. All uncertainties are at the $2\sigma$ level hereafter. The width of the high-velocity component for M2 is systematically greater (by 0.04–0.06 mm/s) than that of the low-velocity component for M2.

The $X_{Fe}^{M1}/X_{Fe}^{M2}$ ratio for each run, listed in Table 2, was taken as the ratio of the sum of area intensities of the outer two peaks (M1) to that of the inner two peaks (M2), assuming as is common practice an identical recoil-free fraction for M1 and M2 sites (Hawthorne, 1983, 1988; Domeneghetti and Steffen, 1992). Uncertainties on the ratios were estimated by propagating the uncertainties on the area intensity of every peak from the fitting. To further verify the assumption for the equality of recoil-free fractions of M1 and M2 sites, we measured two samples at three temperatures of 125, 175 and 225 K (see below).

## 4. EXPERIMENTAL RESULTS

### 4.1. Intracrystalline Fe-Mg Distribution Coefficient ($K_D$)

From the $X_{Fe}^{M1}/X_{Fe}^{M2}$ ratio $r$, $X_{Fe}^{M1}$ is calculated as $rY_{Fe}/(1 + r)$ where $Y_{Fe}$ is the total number of Fe atoms on a four-cation formula unit (i.e., 2 times $X_{Fs}$), $X_{Fe}^{M2}$ is $Y_{Fe} - X_{Fe}^{M1}$, $X_{Fe}^{M1}$ is $1 - Y_1 - X_{Mg}^{M1}$ where $Y_1$ is the sum of all other cations in M1 site (minor Al, Cr, Ti), and $X_{Mg}^{M2}$ is $Y_{Mg} - X_{Mg}^{M1}$. Then $K_D$ is calculated according to Eqn. 2 with Mn and Ca assumed to be totally in the M2 site (Stimpfl, 2005).

The resultant Fe-Mg distribution coefficients are reported in Table 2 and shown in Figure 2a for sample En-LMA and Figure 2b for sample En-82161 in Arrhenius plots. Propagated $2\sigma$ errors of $\ln K_D$ values from spectrum fitting errors are listed in Table 2, which ranges from 0.011 to 0.070 ($2\sigma$). An alternative estimate of the uncertainty in $\ln K_D$ is the reproducibility at each experimental condition, which is somewhat larger than the fitting errors. For example, for En-LMA at 900°C, $\ln K_D$ value is reproducible within an uncertainty of ± 0.077 ($2\sigma$).

The equilibrium Fe-Mg distribution at each temperature is demonstrated by either the convergence of $K_D$ for ordering and disordering experiments (Fig. 3) or the steady state of ordering for runs with different heating duration, or both. Data for sample En-82161 at 1000°C deviate noticeably from the trend defined by $K_D$'s at 600 to 900°C (Fig. 2b). This deviation is likely due to resetting during quenching, and the 1000°C data were not used for further treatment. Although the two samples have different compositions (Table 1), the $K_D$ values for both starting samples at the same temperature (600 to 900°C) are identical within experimental uncertainties. Therefore, we fit all data for both starting samples (En-LMA: 600 to 1000°C; En-82161: 600 to 900°C; Fig. 2c) taking into account individual uncertainties, yielding

$$\ln K_D = 0.391(\pm 0.131) - 2205(\pm 141)/T, \qquad (3)$$

where $T$ is temperature in K, and reported uncertainties are at the $2\sigma$ level. The resultant standard-state enthalpy and entropy changes for the intracrystalline cation exchange reaction, $Fe(M2)Mg(M1)Si_2O_6 = Mg(M2)Fe(M1)Si_2O_6$, are 18(±1) kJ/mol and 3.3(±1.1) J/(mol · K), respectively. The above equation reproduces the experimental temperatures (600 to 1000°C) using individual measurements with a $2\sigma$ uncertainty of 44°C, and a maximum deviation of 55°C (for a run at 1000°C, #5 in Table 2). When $\ln K_D$ values of two to ten experiments at any

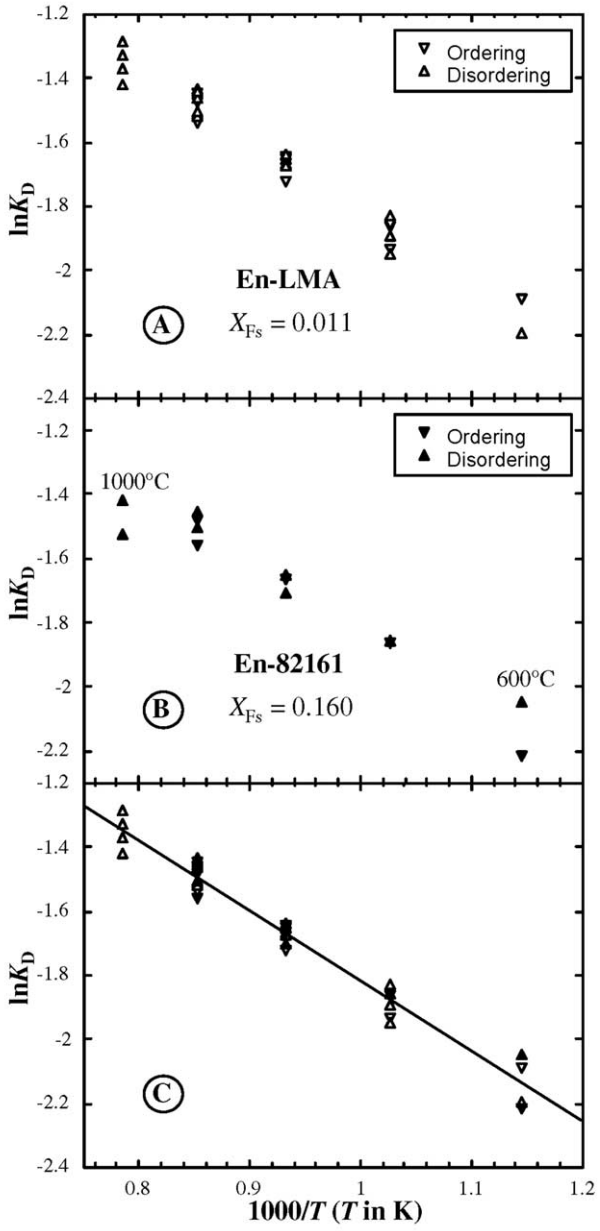


Fig. 2. Relationship between experimentally determined Fe-Mg distribution coefficients ($K_D$) and temperature ($T$) for two starting orthopyroxene crystals. (a) Sample En-LMA. (b) Sample En-82161. (c) $K_D$ data for two orthopyroxene crystals, except those at 1000°C for sample En-821651, which were affected by quenching. The solid line is a linear fit to the data weighted by reproducibility ($\ln K_D = 0.391 - 2205/T$).

given temperature are averaged, the above equation reproduces the experimental temperature to within 8°C.

The calculated apparent equilibrium temperatures using the average $K_D$ values of the two unheated samples are 554°C for sample En-LMA and 325°C for sample En-82161. The much higher temperature recorded for En-LMA suggests it cooled much more rapidly than En-82161. The high rate of cooling of En-LMA is puzzling, but may be related to its formation in a vein.

### 4.2. Kinetic Data

Time series data in this work are useful to demonstrate an approach to equilibrium in our experiments. Such data can also be used to determine the reaction rate coefficient at each temperature assuming a reaction rate law. If reaction 1 is an elementary reaction, the reaction rate law is:

$$\frac{dX_{Fe}^{M1}}{dt} = k_f X_{Fe}^{M2} X_{Mg}^{M1} - k_b X_{Fe}^{M1} X_{Mg}^{M2}, \quad (4)$$

where $k_f$ is the forward reaction rate coefficient (that is, the disordering rate coefficient, $k_{dis}$) of reaction 1, $k_b$ is the backward reaction rate coefficient, and $k_f/k_b = K_D$ (e.g., Mueller, 1969; Ganguly, 1982). Note that this definition of $k_f$ is 2 times that in Kroll et al. (1997). Eqn. 4 predicts a monotonic approach to equilibrium. Isothermal kinetic data were obtained at 600, 700, 800 and 900°C for sample En-LMA. The data, plotted as $X_{Fe}^{M1}$ vs. experimental duration, are shown in Figure 3. The ordering reaction starting with the experimentally disordered orthopyroxene approaches equilibrium monotonically (Fig. 3). However, the disordering reaction starting with unheated orthopyroxene does not. Instead, $X_{Fe}^{M1}$ consistently deviates even further from equilibrium initially and only afterwards approaches equilibrium gradually. This systematic behavior is observed for every temperature, and deviations away from equilibrium are all outside measurement uncertainty. The behavior at 900°C might be due to time needed to heat up the sample, but at other temperatures the behavior persists for a much longer time than the heating-up time (e.g., it persisted for 100 min at 600°C whereas the heating time is <2 min). The observed behavior of deviation away from equilibrium for the order-disorder reaction in orthopyroxene is reminiscent of that observed for the hydrous species reaction in rhyolitic melt (Zhang et al., 1995). The nonmonotonic approach to equilibrium may be due to: (i) oxidation of Fe in M1 site during initial dehydrogenation reaction (Skogby and Rossman, 1989); (ii) the adjustment of the defect population from the natural crystal to experimental fO2-T condition during the early stage of heating; and (iii) nonrandom initial distribution of Fe in M1 site (similar to what Zhang et al., 1995, modeled for hydrous species reaction in rhyolitic melt). It is also possible that reaction 1 is not an elementary reaction. Because the effect of nonmonotonic concentration evolution is only $\sim 5\sigma$, we decided that it is not worth the effort to develop a comprehensive model to constrain the source of the transient effect.

Both the ordering and disordering kinetic data are fit (Fig. 3) to extract the forward reaction rate coefficients $k_f$ (that is, $k_{dis}$, the reaction rate constant for disordering) for reaction 1 at 600, 700, 800, and 900°C by ignoring any possible nonelementariness of the reaction. The data are shown in an Arrhenius plot (Fig. 4). The disagreement of $k_f$ values from the ordering and disordering experiments is significant at 600 and 900°C. If only the monotonic parts of the disordering experiments are fit, the disagreement of $k_f$ values from the ordering and disordering experiments is reduced. Because of the large uncertainty, we decided not to report an Arrhenius equation. The ordering experiments behave more simply and $k_f$ values extracted from them (solid dots in Fig. 4) are expected to be more reliable. Comparison of our kinetic data with the assessed kinetic model

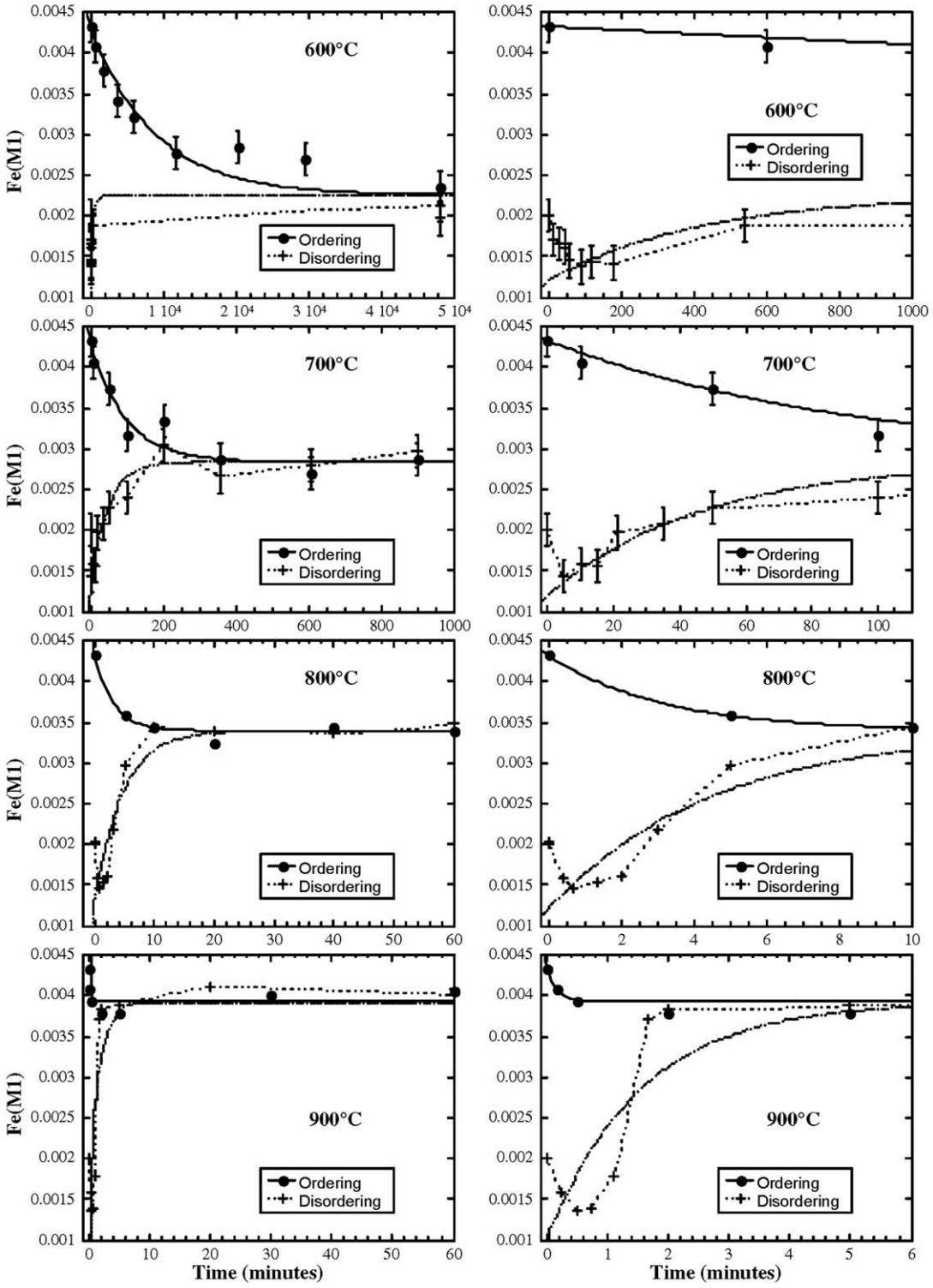


Fig. 3. Kinetic and reversed experiments to demonstrate the approach to equilibrium. The right-hand side displays data at short times to show the nonmonotonic behavior. The ordering experiments are fit (solid curve) to obtain the reaction rate constant. The disordering data are connected by thin dashed curves and are nonmonotonic, but are nonetheless fit (thick dashed curve).

of Kroll et al. (1997) (solid line) shows that there is general agreement. If only the $k_f$ values from the ordering experiments are used, our data show a stronger temperature dependence than the model of Kroll et al. (1997). At 800 to 900°C, our data agrees well with their model, but the disagreement becomes significant as temperature decreases.

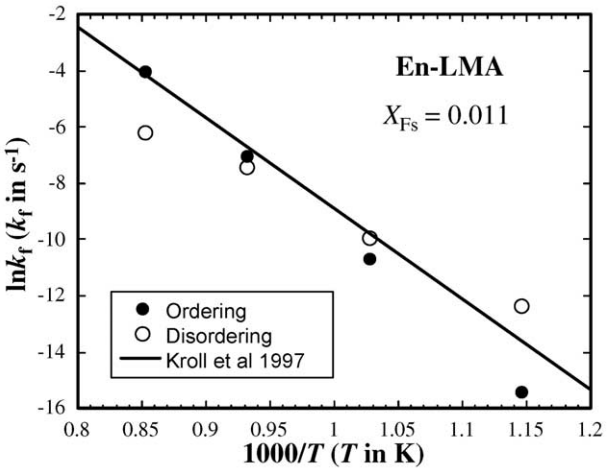


Fig. 4. Arrhenius plot of the reaction rate coefficient. The solid circles are for $k_f$ (i.e., $k_{dis}$) extracted from the ordering experiments. The open circles are for $k_f$ extracted from the disordering experiments. For the disordering experiments, Fe(M1) versus time is not monotonic, and hence the extracted $k_f$ values are of questionable significance. Because the data show much scatter, no fit is given. The solid line is calculated from Kroll et al. (1997) for $X_{Fs} = 0.011$.

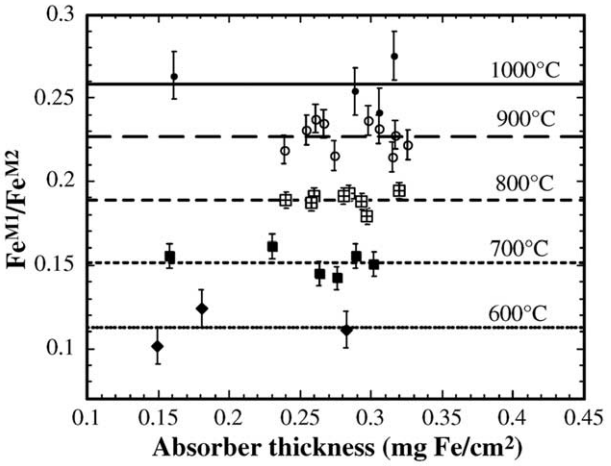


Fig. 5. Relationship between determined $Fe^{M1}/Fe^{M2}$ ratio and average Mössbauer absorber thickness for sample En-LMA. No significant dependence was observed. Lines through data points are horizontal guide lines representing the average ratio at each temperature.

### 4.3. Potential Complications

#### *4.3.1. Effects of Thickness and Nonuniform Absorber*

The thickness effect (the saturation of transmitted absorption peaks) is a well-known feature of Mössbauer spectroscopy (Bancroft et al., 1967; Bancroft, 1973; Rancourt, 1989; Rancourt et al., 1993). It results in an accentuation of weak peaks relative to strong peaks and becomes more significant as areal differences between spectral components increase. The problem stems from the lack of standard Mössbauer procedures to address the Beer-Lambert law (Dunham et al., 1993). One experimental study (Skogby et al., 1992) showed that the thickness effect caused an overestimation of Fe in the M1 site by ~2% of total Fe for an absorber thickness of 5 mg Fe/cm$^2$. Errors in measured site occupancies for Mg-rich orthopyroxenes tend to be larger than those for more Fe-rich samples. In the present study, the average absorber thicknesses (0.15–0.44 mg Fe/cm$^2$) are far smaller than those commonly used and assumed as thin absorbers in previous studies (i.e., 2–5 mg Fe/cm$^2$). The calculated $X_{Fe}^{M1}/X_{Fe}^{M2}$ ratios at a given temperature for our data are independent of average absorber thickness (Fig. 5), suggesting that the thickness effect is insignificant for the range of thickness that were used. In conclusion, the thickness effect is negligible in this study.

The effect of a nonuniform absorber has been examined in previous studies, and it can cause significant overestimation of Fe in M1 (e.g., Anovitz, 1987). Mössbauer absorbers prepared from the powdered orthopyroxene samples are commonly assumed to have a uniform effective thickness. However, orthopyroxene has strong {110} cleavages, and the property will likely result in stacking or packing imperfections in the absorbers. This may be effectively modeled as if there are "holes" in the absorber such that part of the gamma ray beam passes through the absorber without encountering the orthopyroxene sample. This effect is minimized by using exceedingly thin absorbers (Moon et al., 1996), such as in the current study. The distribution of Fe was tested in a test run (run #73a, Table 2) in which the absorber consisted of half of the absorber in run #73 and hence contained more "holes," did not deviate significantly from that in run #73. Furthermore, runs using different absorber thickness, which are equivalent to nonuniform absorbers, also yield consistent results (Fig. 5). In conclusion, the effect of nonuniform absorber is negligible.

#### *4.3.2. Effect of Oxidation*

Since the distribution of Mg between M1 and M2 sites was calculated based on the determined $X_{Fe}^{M1}/X_{Fe}^{M2}$ ratios and total Fe in orthopyroxene, ignoring the oxidation of Fe to $Fe^{3+}$ could cause uncertainties in calculated $K_D$. One potential process for the oxidation of Fe is reaction between orthopyroxene and oxygen in the $N_2$ atmosphere ($f_{O2} \approx 10^{-5}$ bar) during heating. This was minimized by using samples consisting of mm-sized grains instead of powdered orthopyroxene. The defect population likely reached equilibrium for the starting composition prepared by disordering the sample at 1000°C, but oxygen diffusion probably did not reach significant depth inside the mm-sized grains. The second process by which Fe may be oxidized is through dehydrogenation during heating if the starting sample contained an appreciable amount of the hydrous component (i.e., $OH^-$) (Skogby and Rossman, 1989; Skogby et al., 1990). No detectable $Fe^{3+}$ (i.e., $<$ 1% of total Fe) was observed from the Mössbauer spectra for any unheated or heat-treated sample in the present study. If a small amount of Fe was oxidized during heat treatment due to the dehydrogenation reaction, the presence of such a small amount of $Fe^{3+}$ below the detection limit of MS may contribute to the kinetic transient observed in the disordering transient and contributes only insignificant uncertainties in the measured $K_D$.

#### *4.3.3. Recoil-Free Fractions*

To investigate the validity of the assumption of equality of the recoil-free fractions on M1 and M2 sites, two samples (#94

and #95) were run at three temperatures, 125, 175, and 225 K. The M1/M2 area ratio obtained at 125 K and 175 K are in agreement within 2% relative in one case and within 3% relative in the other case, about the same as fitting uncertainties and better than interexperimental reproducibility. As measurement temperature increases, it becomes progressively more difficult to resolve M1 peaks from M2 peaks and the fitting precision therefore declines. At 225 K, resolution of M1 from M2 peaks is very poor, but an algorithm constraining the area ratio of M1/M2 to be the same as that at 125 K does fit the data well. Based on data at different temperatures, we conclude that the area ratio of M1 to M2 sites is indeed independent of measurement temperature, and hence the assumption of equality of the M1 and M2 site recoil-free fractions is appropriate. The conclusion is consistent with that reached by Van Alboom et al. (1993) with more extensive data.

#### 4.3.4. *Effect of Quenching*

If the intrasite kinetics are sufficiently rapid, the ordering state obtained at high temperatures may be reset during quenching (Anovitz et al., 1988). To evaluate this effect, comparative experiments were run at 900 and 1000°C for sample En-LMA with different quenching procedures (Table 2). Samples that were quenched in water and in air gave similar results within experimental uncertainties at each temperature. Therefore, we conclude that the quenching effect was negligible for all runs for sample En-LMA. For sample En-82161, runs at 900 and 1000°C were all quenched in water, but the $K_D$ values at 1000°C lie off the trend defined by the En-82161 data at lower temperatures (Fig. 2b), and hence the ordering states were likely reset during quenching. To examine whether it is due to a transitional structural state as was observed in a synthetic orthopyroxene (sample Fs25; Yang and Ghose, 1994), a powder XRD pattern was obtained and it revealed no significant difference in the diffraction pattern for the starting material and the heat-treated sample. Therefore, quenching is likely the cause of the anomalous behavior of $K_D$ at 1000°C for sample En-82161. Using Eq. (3), the apparent equilibrium temperatures calculated from the average $K_D$ for the two experimental samples at 1000°C is 911°C, significantly lower than the experimental temperature.

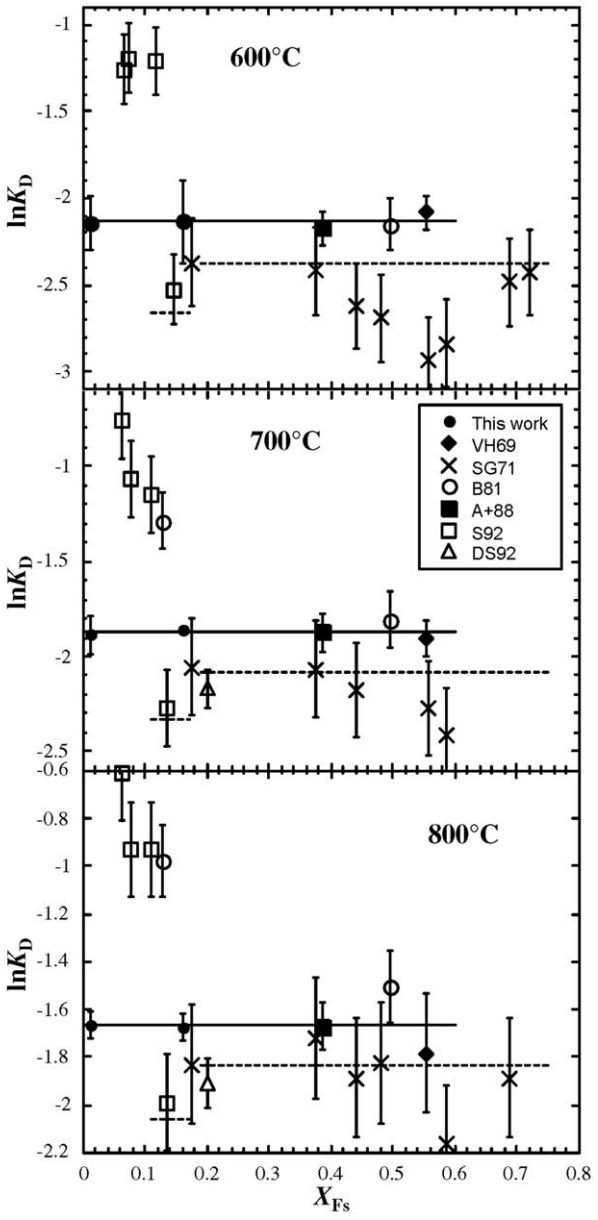


Fig. 6. $K_D$ as a function of temperature and orthopyroxene composition from Mössbauer measurements. Data sources: VF69, Virgo and Hafner (1969); SG71, Saxena and Ghose (1971); B81, Besancon (1981); A+88, Anovitz et al. (1988); S92, Skogby (1992); DS92, interpolated from Domeneghetti and Steffen (1992). The dashed lines (two lines in each panel) are calculated from the calibration of Stimpfl et al. (1999) based on XRD data. The thick solid line represents the compositionally independent $K_D$ model adopted in this study.

## 5. DISCUSSION

### 5.1. Comparison with Previous Mössbauer Equilibrium Studies

Several studies have been conducted to investigate Fe-Mg order-disorder in orthopyroxenes using conventional Mössbauer spectroscopy (Virgo and Hafner, 1969; Saxena and Ghose, 1971; Besancon, 1981; Anovitz et al., 1988; Domeneghetti and Steffen, 1992; Skogby, 1992). The Fe-Mg distribution coefficients from these studies have been recalculated based on the reported site occupancies to account for the minor elements following the same procedure as in this study. Data from Virgo and Hafner (1969) were also adjusted according to reported Mössbauer line widths (the original Fe distributions were calculated based on the linear intensities, not area intensities). The results, together with those from this study, are plotted in Figure 6. Only 600 to 800°C data are examined because experiments at lower temperature probably did not attain equilibrium (Besancon, 1981; Anovitz et al., 1988) and higher temperature data might have been reset during quench especially for $X_{Fs} > 0.2$. Data obtained on samples with $X_{Fs} > 0.8$ are not shown because such samples are unstable at ambient pressure and may break down to olivine + quartz during prolonged heating, leading to anomalous $K_D$ behavior (Anovitz et al., 1988).

The following observations can be made based on Möss-

bauer data in Figure 6. Data from the University of Michigan for three orthopyroxene compositions, $X_{Fs} = 0.011$ (this study), $X_{Fs} = 0.16$ (this study) and $X_{Fs} = 0.39$ (Anovitz et al., 1988) show that $K_D$ is independent of composition at $X_{Fs} \leq 0.4$. Mössbauer data from other labs are more scattered. Among these, $K_D$ values for $X_{Fs} \leq 0.2$ (Besancon, 1981; Domeneghetti and Stefen, 1992; Skogby, 1992) are either too high or too low, attributable to difficulties of conventional MS to determine $K_D$ for low-Fe orthopyroxenes. Among $K_D$ values for $X_{Fs} > 0.2$, those by Virgo and Hafner (1969) and Besancon (1981) are consistent with our data and support a $K_D$ that is independent of composition for $X_{Fs} \leq 0.6$; but those of Saxena and Ghose (1971), which comprise the largest MS data set, are more scattered and are generally smaller than our $K_D$ values. It is not clear why the data of Saxena and Ghose (1971) differ from most other Mössbauer data.

Based on data shown in Figure 6, our assessment is that the $K_D$ for Fe-Mg order-disorder reaction in orthopyroxene is independent of Fe and Mg content, at least for Fs ≤60%. It is further inferred that the $K_D$ is also independent of Fe and Mg content even for Fs >60% and that previous data showing a compositional dependence were either compromised by the difficulty of measurements or by the instability of Fe-rich orthopyroxene (Anovitz et al., 1988). Zema et al. (2003) showed that the presence of Ca does not seem to affect the $K_D$. The conclusion that $K_D$ is independent of composition to a good approximation will simplify future treatments of this reaction and its application as a geospeedometer.

### 5.2. Comparison with Previous XRD Equilibrium Studies

Single-crystal XRD techniques have also been applied to studies of Fe-Mg order-disorder in orthopyroxenes (Yang and Ghose, 1994; Kirfel, 1996; Kroll et al., 1997; Stimpfl et al., 1999; Schlenz et al., 2001). Yang and Ghose (1994) carried out an in situ order-disorder study and modeled $K_D$ values as a function of $X_{Fs}$ with a regular solution model. Kirfel (1996) conducted an interlaboratory study and documented some inconsistencies. Kroll et al. (1997) provided a critical review of the XRD studies and again modeled $K_D$ values as a function of $X_{Fs}$ with a regular solution model. Stimpfl et al. (1999) reported a comprehensive new study of the equilibrium fractionation, reviewed literature XRD data, and adopted $K_D$ as a step function of $X_{Fs}$ at each temperature: one $K_D$ value for the $X_{Fs}$ range of 0.19 to 0.75, and another lower value for the $X_{Fs}$ range of 0.11 to 0.17 (Fig. 6). They considered whether the anomalously low $K_D$ at $X_{Fs}$ of 0.11 to 0.17 is real, or whether it is related to inherent problems in the XRD technique at low $X_{Fs}$. The XRD data of Schlenz et al. (2001) are consistent with the model of Stimpfl et al. (1999).

There are two main differences between our MS results and above XRD results. One is that our high-sensitivity Mössbauer results combined with literature data indicate that $K_D$ is independent of $X_{Fs}$ at $X_{Fs}$ range of 0.01 to 0.6, whereas XRD results indicate that $K_D$ for $X_{Fs}$ of 0.11 to 0.17 is significantly lower than that in the $X_{Fs}$ range of 0.19 to 0.75. The step-function dependence of $K_D$ on $X_{Fs}$ does not have any theoretical basis, and is most likely an artifact of the XRD method. The persistence of low $K_D$ values for magnesian orthopyroxenes, compared with hypersthenes of intermediate $X_{Fs}$, seems to indicate a systematic pitfall in the XRD methodology. Old Mössbauer data, on the other hand, indicate a high $K_D$ at low $X_{Fs}$, opposite to the trend of the XRD data. The most obvious explanation is that both results are questionable due to measurement errors. Hence, we suggest that the equation derived for the $X_{Fs}$ range of 0.19 to 0.75 by Stimpfl et al. (1999), $\ln K_D = 0.547 - 2557/T$, is applicable to the entire orthopyroxene composition for XRD investigations.

The second difference between our MS results and recent XRD results is the systematic difference on the absolute values of $K_D$ (Fig. 6) and in terms of the temperature dependence ($\Delta H^0_{exch}$). The $K_D$ values obtained at a given temperature in XRD studies are consistently lower than those determined in the current study, and the differences are outside measurement errors. The reason for the systematic deviation is not clear. Previous studies to evaluate the differences between MS and XRD methods were inconclusive (Domeneghetti and Steffen, 1992; Skogby et al., 1992). The systematic difference means that one cannot mix results from the two methods. Nonetheless, applied consistently, each method (MS or XRD) could be used to infer apparent equilibrium temperature and cooling rates.

### 5.3. Comparison with Previous Kinetic Studies

Figure 4 compares our kinetic rate constants with the formulation of Kroll et al. (1997) who critically evaluated and refit all original kinetic data from both Mössbauer and XRD methods. Although our data are scattered, there is general agreement with the constants of Kroll et al. (1997). New kinetic data by Schlenz et al. (2001) are also consistent with the formulation of Kroll et al. (1997). It might be a surprise that there is less agreement in the equilibrium $K_D$ values than in the kinetic rate constants $k_f$. One reason is that $k_f$ values from Mössbauer and XRD methods are consistent because $k_f$ is a measure of the time scale to reach equilibrium and hence is independent of the accurate calibration of the site distribution. The second reason is that higher accuracy is required for $K_D$ than for $k_f$ in geospeedometry applications because the variation of $K_D$ is small.

## 6. CONCLUSIONS

The equilibrium distribution of Fe and Mg between the M1 and M2 sites in orthopyroxene has been measured at 1 atm and 600 to 1000°C for two magnesian orthopyroxene crystals ($Fs_1$ and $Fs_{16}$) using a high-sensitivity Mössbauer spectrometer. The most important conclusion from this study is that the Fe-Mg distribution coefficients ($K_D$) are independent of orthopyroxene composition within experimental uncertainty, and that $K_D$ values from Mössbauer method can be described as a function of temperature by a single equation: $\ln K_D = 0.391(\pm 0.131) - 2205(\pm 141)/T$, where $T$ is temperature in K, and uncertainties are at the $2\sigma$ level. Strongly nonideal mixing models for Fe-Mg mixing between octahedral sites in magnesian orthopyroxenes, which were required by earlier work are unnecessary. Kinetic parameters derived from Mössbauer measurements are in good agreement with that obtained from XRD data. $K_D$ values determined by

Mössbauer method are, however, significantly larger than those by the XRD technique. Furthermore, the anomalous variation of $K_D$ for magnesian orthopyroxenes in the XRD data are likely an analytical artifact.

*Acknowledgments*—We are grateful to L. M. Anovitz of Oak Ridge National Laboratory and G. Harlow of the American Museum of Natural History at New York for donating orthopyroxene crystals. We thank J. Becket, J. Chen, J. Ganguly, F. C. Hawthorne, D. G. Rancourt, S. K. Saxena, D. J. Weidner, J. Zhang and an anonymous reviewer for comments and discussion. J. Granguly is also thanked for calculating the statistically most probable formula. This research was partially supported by grants from NSF (EAR 94-58368, 97-06107, 01-25506, and 02-28752), the Department of Geological Sciences of the University of Michigan, the Geological Society of America, and the Mineral Physics Institute at SUNY Stony Brook.

*Associate editor:* B. Mysen

## REFERENCES

Angel R. J., McCammon C., and Woodland A. B. (1998) Structure, ordering and cation interactions in Ca-free $P2_1/c$ clinopyroxenes. *Phys. Chem. Minerals* **25,** 249–258.

Anovitz L. M. (1987) Pressure-temperature-time constraints on the metamorphism of the Grenville Province, Ontario. Ph.D. diss., University of Michigan, Ann Arbor.

Anovitz L. M., Essene E. J., and Dunham W. R. (1988) Order-disorder experiments on orthopyroxenes: Implications for the orthopyroxene geospeedometer. *Am. Mineral.* **73,** 1060–1073.

Bancroft G. M. (1973) *Mössbauer Spectroscopy. An Introduction for Inorganic Chemists and Geologists*. McGraw-Hill.

Bancroft G. M., Burns R. G., and Maddock A. G. (1967) Determination of the cation distribution in the cummingtonite-grunerite series by Mössbauer spectroscopy. *Am. Mineral.* **52,** 1009–1026.

Besancon J. R. (1981) Rate of cation disordering in orthopyroxenes. *Am. Mineral.* **66,** 965–973.

Burnham C. W., Ohashi Y., Hafner S., and Virgo D. (1971) Cation distribution and atomic thermal vibrations in an iron-rich orthopyroxene. *Am. Mineral.* **56,** 850–876.

Domeneghetti M. C. and Steffen G. (1992) M1, M2 site populations and distortion parameters in synthetic Mg-Fe orthopyroxenes from Mössbauer spectra and X-ray structure refinements. *Phys. Chem. Minerals* **19,** 298–306.

Domeneghetti M. C., Molin G. M., Triscari M., and Zema M. (2000) Orthopyroxene as a geospeedometer: Thermal history of Kapoeta, Old Homestead 001 and Hughes 002 howardites. *Meteor. Planet. Sci.* **35,** 347–354.

Dunham W. R., Harding L. J., and Sands R. H. (1993) Mössbauer spectroscopy of metalloproteins and the use of Fourier transforms. *Eur. J. Biochem.* **214,** 1–8.

Ganguly J. (1982) Mg-Fe order-disorder in ferromagnesian silicates: II. Thermodynamics, kinetics and geological applications. In *Advances in Physical Geochemistry*, vol. 2 (ed. S. K. Saxena), pp. 58–99. Springer-Verlag.

Ganguly J., Yang H., and Ghose S. (1994) Thermal history of mesosiderites: Quantitative constraints from compositional zoning and Fe-Mg ordering in orthopyroxenes. *Geochim. Cosmochim. Acta* **58,** 2711–2723.

Ganguly J. and Domeneghetti M. C. (1996) Cation ordering of orthopyroxenes from the Skaergaard Intrusion: Implications for the subsolidus cooling rates and permeabilities. *Contrib. Mineral. Petrol.* **122,** 359–367.

Ghose S. (1965) $Mg^{2+}$-$Fe^{2+}$ order in an orthopyroxene, $Mg_{0.93}Fe_{1.07}Si_2O_6$. *Zeit. Kristal.* **122,** 81–99.

Ghose S. and Hafner S. (1967) $Mg^{2+}$-$Fe^{2+}$ distribution in metamorphic and volcanic orthopyroxenes. *Zeit. Kristal.* **125,** 1–6.

Hawthorne F. C. (1983) Quantitative characterization of site-occupancies in minerals. *Am. Mineral.* **68,** 287–306.

Hawthorne F. C. (1988) Mössbauer spectroscopy. *Rev. Mineral.* **18,** 255–340.

Heinemann R., Kroll H., Langenhorst F., and Lueder T. (2000) Time and temperature variation of the intracrystalline $Fe^{2+}$, Mg fractionation in Johnstown meteoritic orthopyroxene. *Eur. J. Mineral.* **12,** 163–176.

Kirfel A. (1996) Cation distributions in olivines and orthopyroxenes: An interlaboratory study. *Phys. Chem. Minerals* **23,** 503–519.

Kroll H., Lueder T., Schlenz H., Kirfel A., and Vad T. (1997) The $Fe^{2+}$, Mg distribution in orthopyroxene: A critical assessment of its potential as a geospeedometer. *Eur. J. Mineral.* **9,** 705–33.

Molin G. M., Saxena S. K., and Brizi E. (1991) Iron-magnesium order-disorder in an orthopyroxene crystal from the Johnstown meteorite. *Earth Planet. Sci. Lett.* **105,** 260–265.

Moon N., Coffin C. T., Steinke D. C., Sands R. H., and Dunham W. R. (1996) A high-sensitivity Mössbauer spectrometer facilitates the study of iron proteins at natural abundance. *Nucl. Instr. Meth.* **B119**, 555–564.

Mueller R. F. (1969) Kinetics and thermodynamics of intracrystalline distributions. Special Paper 2, pp. 83–93. Mineralogical Society of America.

Rancourt D. G. (1989) Accurate site populations from Mössbauer spectroscopy. *Nucl. Instr. Meth.* **B44**, 199–210.

Rancourt D. G., McDonald A. M., Lalonde A. E., and Ping J. Y. (1993) Mössbauer absorber thickness for accurate site populations in Fe-bearing minerals. *Am. Mineral.* **78,** 1–7.

Saxena S. K. and Ghose S. (1971) $Mg^{2+}$-$Fe^{2+}$ order-disorder and the thermodynamics of the orthopyroxene crystalline solution. *Am. Mineral.* **56,** 532–559.

Saxena S. K., Domeneghetti M. C., Molin G. M., and Tazzoli V. (1989) X-ray diffraction study of $Fe^{2+}$-Mg order-disorder in orthopyroxene: Some kinetic results. *Phys. Chem. Minerals* **16,** 421–427.

Schlenz H., Kroll H., and Phillips M. W. (2001) Isothermal annealing and continuous cooling experiments on synthetic orthopyroxenes: Temperature and time evolution of the Fe, Mg distribution. *Eur. J. Mineral.* **13,** 715–726.

Seifert F. (1983) Mössbauer line-broadening in aluminous orthopyroxenes: Evidence for next-nearest-neighbour interactions and short-range order. *N. Jahrb. Mineral. Abh.* **148,** 141–162.

Shi P., Saxena S. K., and Sundman B. (1992) Sublattice solid solution model and its application to orthopyroxene $(Mg, Fe)_2Si_2O_6$. *Phys. Chem. Minerals* **18,** 393–405.

Skogby H. (1992) Order-disorder kinetics in orthopyroxenes of ophiolite origin. *Contrib. Mineral. Petrol.* **109,** 471–478.

Skogby H. and Rossman G. R. (1989) $OH^-$ in pyroxene: An experimental study of incorporation mechanisms and stability. *Am. Mineral.* **74,** 1059–1069.

Skogby H., Bell D. R., and Rossman G. R. (1990) Hydroxide in pyroxene: Variations in the natural environment. *Am. Mineral.* **75,** 764–774.

Skogby H., Annersten H., Domeneghetti M. C., Molin G. M., and Tazzoli V. (1992) Iron distribution in orthopyroxene: A comparison of Mössbauer spectroscopy and X-ray refinement results. *Eur. J. Mineral.* **4,** 441–452.

Stimpfl M. (2005) The Mn, Mg-intracrystalline exchange reaction in donpeacorite ($Mn_{0.54}Ca_{0.03}Mg_{1.43}Si_2O_6$) and its relation to the fractionation behavior of Mn in Fe, Mg-orthopyroxene. *Am. Mineral.* **90,** 155–161.

Stimpfl M., Ganguly J., and Molin G. M. (1999) $Fe^{2+}$-Mg order-disorder in orthopyroxene: Equilibrium fractionation between the octahedral sites and thermodynamic analysis. *Contrib. Mineral. Petrol.* **136,** 297–309.

Van Alboom A., De Grave E., and Vandenberghe R. E. (1993) Study of the temperature dependence of the hyperfine parameters in two pyroxenes by $^{57}$Fe Mossbauer spectroscopy. *Phys. Chem. Minerals* **20,** 263–275.

Virgo D. and Hafner S. (1969) $Fe^{2+}$, Mg order-disorder in heated orthopyroxenes. Special Paper 2, pp. 67–81. Mineralogical Society of America.

Virgo D. and Hafner S. (1970) $Fe^{2+}$-Mg order-disorder in natural orthopyroxenes. *Am. Mineral.* **55,** 201–223.

Wang L. (1999) Mineralogical and petrological study of pyrope megacrysts and related minerals from the Four Corners area, Colorado Plateau, and an experimental study of Fe-Mg order-disorder

in magnesian orthopyroxenes. Ph.D. diss., University of Michigan, Ann Arbor.

Xu Z. and Zhang Y. (2002) Quench rates in water, air and liquid nitrogen and inference of temperature in volcanic eruption columns. *Earth Planet. Sci. Lett.* **200,** 315–330.

Yang H. and Ghose S. (1994) In-situ Fe-Mg order-disorder studies and thermodynamic properties of orthopyroxene $(Mg,Fe)_2Si_2O_6$. *Am. Mineral.* **79,** 633–643.

Zema M., Domeneghetti M. C., and Molin G. M. (1996) Thermal history of Acapulco and ALHA81261 acapulcoites constrained by $Fe^{2+}$-Mg ordering in orthopyroxene. *Earth Planet. Sci. Lett.* **144,** 359–367.

Zema M., Tarantino S. C., Domeneghetti M. C., and Tazzoli V. (2003) Ca in orthopyroxene: Structural variations and kinetics of the disordering process. *Eur. J. Mineral.* **15,** 373–380.

Zhang Y. (1994) Reaction kinetics, geospeedometry and relaxation theory. *Earth Planet. Sci. Lett.* **122,** 373–391.

Zhang Y., Stolper E. M., and Ihinger P. D. (1995) Kinetics of reaction $H_2O + O = 2OH$ in rhyolitic glasses: Preliminary results. *Am. Mineral.* **80,** 593–612.